Steady-State D-^{3}He Proton Production in an IEC Fusion Device

R.P. Ashley, G.L. Kulcinski, J.F. Santarius, S. Krupakar Murali, G. Piefer, R. Radel

October 2000

UWFDM-1144

Presented at the 14th Topical Meeting on the Technology of Fusion Energy, October 15–19, 2000, Park City UT

FUSION TECHNOLOGY INSTITUTE

UNIVERSITY OF WISCONSIN

MADISON WISCONSIN

STEADY-STATE D^3He PROTON PRODUCTION IN AN IEC FUSION DEVICE

R. P. Ashley, G. L. Kulcinski, J. F. Santarius,
S. Krupakar Murali, G. Piefer, and R. Radel
University of Wisconsin-Madison, Fusion Technology Institute
1500 Engineering Drive
Madison WI 53706
(608) 263-2352

ABSTRACT

Inertial electrostatic confinement of ions has been successfully used to achieve conditions necessary for the fusion of advanced fuels, such as ^3He. This type of device at the University of Wisconsin was the first to produce steady-state D^3He fusion, and has since produced up to 7 x 10^6 14.7 MeV proton/s from the D^3He fusion reaction. The factors influencing the reaction rate and the experimental results are discussed.

I. INTRODUCTION

The fusion reaction,

$$D + {}^3He \rightarrow p\ (14.7\ MeV) + {}^4He\ (3.7\ MeV) \qquad (1)$$

produces high-energy protons that are potentially very useful in a number of applications. The production of short-lived medical isotopes on-site, such as ^{15}O or ^{18}F requires a device that can produce protons above 3 MeV and would benefit significantly from being portable.[1-3] Fusion power production using advanced fuels has much less of a problem with neutron activation and may be able to use direct energy conversion.[4-5] Space propulsion requires a low mass power plant without the requirement for large amounts of shielding. All applications benefit greatly by the ability to run in a steady-state mode. The IEC device has produced advanced fuel fusion and shown substantial progress in increasing the reaction rate.[6-9]

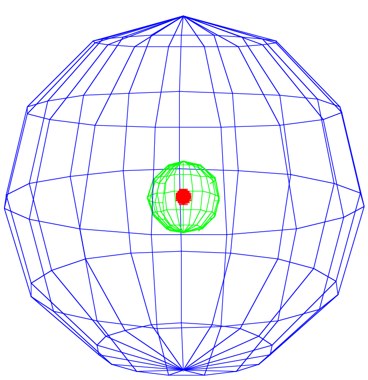

Figure 1. Spherical grid geometry of an Inertial Electrostatic Confinement (IEC) device.

II. THEORY OF OPERATION

Gridded inertial electrostatic devices rely on the radial acceleration of charged particles between concentric, nearly transparent electrodes (Figure 1).[10-16] For typical grid spacing of 0.1-1 m, 10's-100's of kV can be sustained between the grids, and the energy of ions accelerated by such potential differences leads to substantial fusion cross sections. A key benefit of IEC fusion lies in the relative ease of achieving high-energy ions compared to producing high temperatures in Maxwellian plasmas, where much of the input energy sustains relatively useless low-energy ions and electrons. The difficulty with IEC fusion stems from space-charge effects that limit the plasma density to low values except near the center of the device, where radial focusing gives very high density in a small volume. Unresolved questions also exist regarding sustaining the IEC core against collisions.[17-20] A gridless IEC variant, called the Polywell™, invokes magnetostatic containment of injected high-energy electrons in a cusped magnetic field to form the electrostatic well.[21] Another type of IEC uses cylindrical grid geometry, which can create a linear converged core.[13]

Achieving a highly converged core remains an eventual goal that probably will be necessary for high-Q (fusion power/input power) operation. The present gridded IEC experiment, however, operating in a somewhat different mode, generates fusion protons and neutrons at relevant levels for creating radioisotopes applicable to nuclear medicine. In this mode, the background neutral gas pressure is relatively high, typically a few mtorr. The mean free path of an accelerated ion against charge exchange at these pressures is on the order of or somewhat larger than the device dimensions. A typical ion then passes one to a few times through the core before charge exchanging with a cold neutral, but the ion usually charge exchanges before it fuses with another ion in the core or collides with a grid wire.

The three fusion reactions that have been studied in an IEC device are D^3He (Eq. 1), DD (Eq. 2), and D-T (Eq. 3).[22]

$$D + D \rightarrow {}^{0}n\ (2.5\ MeV) + {}^{3}He\ (0.8\ MeV) \quad 50\% \quad (2)$$
$$\rightarrow {}^{1}H\ (3\ MeV) + T\ (1\ MeV) \quad 50\%$$
$$D + T \rightarrow {}^{0}n\ (14.1\ MeV) + {}^{4}He\ (3.5\ MeV) \quad (3)$$

Figure 2 shows the reaction rates for fusion in the converged core (D^{+1}+D^{+1} and D^{+1}+$^{3}He^{+1}$) and for fusion by a charge-exchange (CX) neutral on the background gas.

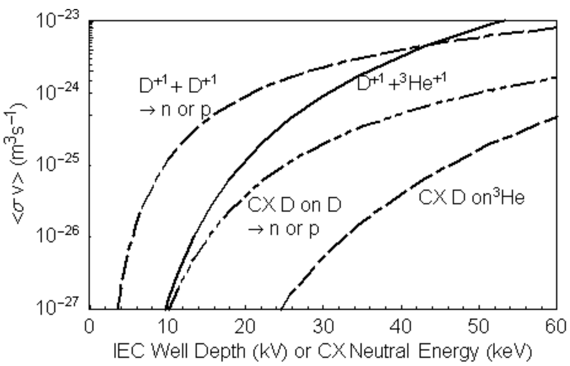

Figure 2. Predictions of key fusion reactions that might occur in the Wisconsin IEC experiment.

The plasma/gas mixture is typically 0.01-0.1% ionized and expected to be predominantly deuterium, because Penning collisions cause D to drain He energy before the He can ionize.[22] Although the core reaction rates are higher, the fusion-product production must be corrected for the density ratio of the species and integrated over the relevant volume, and the chamber is much bigger than the ~1 cm^3 core. In the present operating range of 30-70 kV potential difference on the grids, the measured ratios of proton production are consistent with CX deuterons fusing with background neutral gas but not consistent with the core dominating the fusion rate.

III. THE WISCONSIN IEC EXPERIMENTAL FACILITY

The facility (Figure 3) consists of a 91 cm diameter cylindrical aluminum vacuum chamber, which is 65 cm tall. This is the same chamber described in earlier work.[23-25]

A 450 l/s turbo pump pumps the chamber down to a base pressure of 2 x 10^{-7} torr. The inner cathode is a 10 cm diameter coarse grid sphere of 0.8 mm tungsten wire supported on a 100 kV vacuum feedthrough. The tungsten construction of the inner grid has allowed operation at input power levels exceeding 8.5 kW without failure. Normal operating voltages range from -25 to -70 kV at 30-150 mA. The power supply used in the present experiments can deliver 75 kV. The outer anode grid is 45 cm in diameter made of stainless steel wire that can be biased with variable amplitude AC and DC voltages. The variable AC bias is used to control the ionization of the fuel gas, which in turn controls the current to the cathode grid. This allows far better control of the ion current and produces a more uniform, higher level of ionization compared to previously used filament ion sources.[23-25] Electronically controlled gas flow regulators adjust the fuel flow ratio and amount into the system. A remote controlled throttle on the turbo pump is used to control the operating pressure of the gas mix. A Residual Gas Analyzer (RGA) is used to monitor the ratio of the fuels present as well as impurity levels.

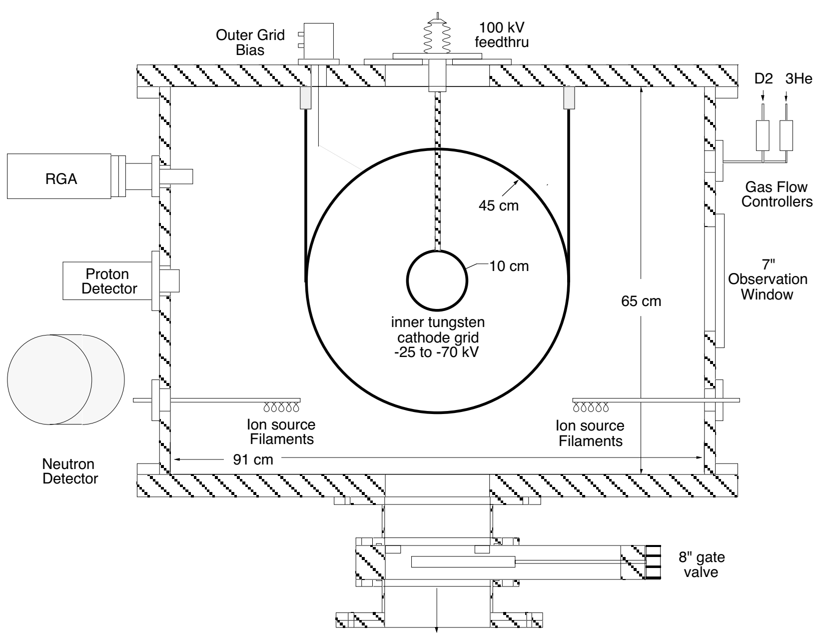

Figure 3. The Wisconsin IEC chamber.

The DD and D^3He reactions produce a steady stream of neutrons, protons, electrons, helium-4 and tritium ions, gammas, and x-rays. The diagnostics currently in use detect the 2.45 MeV neutron from the D-D reaction, the 3 MeV proton from the D-D reaction, and the 14.7 MeV proton from the D^3He reaction. The proton detector used is a Canberra Passivated Implanted Planar Silicon (PIPS) Detector. It is mounted inside a 6 cm diameter water-cooled tube on the side of the chamber 80 cm from the center. This solid-state silicon detector has an active area of 1200 mm^2 and a depletion region thickness of 700 μm. This thickness allows both the 3 MeV proton and the 14.7 MeV proton to be detected at the same time. A 25 μm thick lead foil is placed in front of the detector to block x-rays and alpha particles, which create unwanted signals in the detector. The detected energy levels of the protons after they pass through the lead are calculated using stopping powers tabulated in the National Institute of Standards and Technology's PSTAR database[26] shown in Figure 4. The measured proton peaks corresponds closely to the calculated values of 1.9 MeV and 5 MeV.

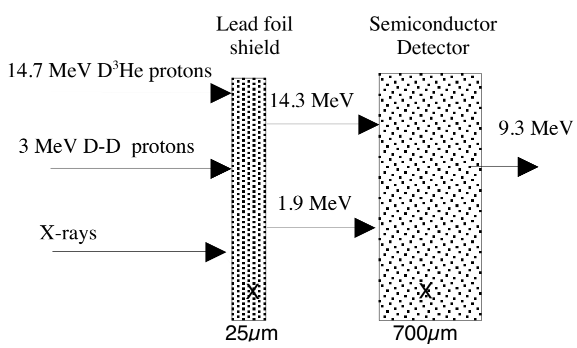

Figure 4. The Pb foil in front of the proton detector shields the unit from x-rays while lowering the energy of the protons from the plasma.

A helium proportional counter neutron detector, placed 90 cm from the center, is used to detect the low-energy neutrons from the D-D reaction. It is mounted outside the chamber in a container of polyethylene to thermalize the neutrons.

The neutron detector was calibrated by placing a Pu-Be source of 2.18 x 10^6 n/s inside the chamber. Although it is expected that the fusion reactions produce a volume source of neutrons, the Pu-Be source is a point source. However, mathematical modeling shows that the detected neutron rate difference between a volume and a point source would be only 5% for the neutron detector.

The proton detector was checked using a ^{241}Am alpha source to determine its efficiency and energy peak location on the multi-channel analyzer. Correction factors were determined by calculating its solid angle view of the volume source of protons. Both the neutron and proton detectors, with their associated signal conditioners, provide a continuous readout of the count rate during the steady-state operation.

IV. EXPERIMENTAL RESULTS

The main factors that affect the fusion reaction rates that have been studied are the fueling conditions and the geometry and biasing of the grids. The inner grid potential has the most influence on the reaction rate. The rate has a near exponential dependence on the voltage, as seen in Figure 5. This is due to the exponential cross-section dependency on the kinetic energy.

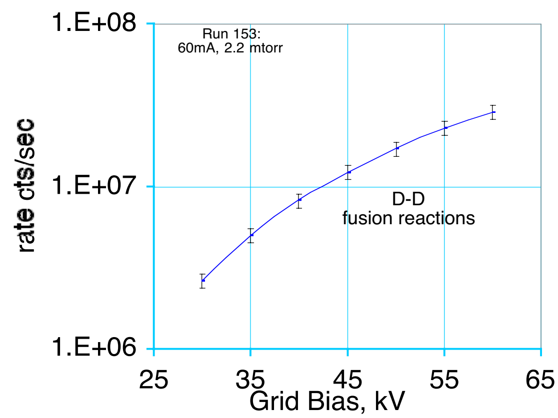

Figure 5. The rate of DD fusion reactions increases rapidly for modest increases in cathode voltage.

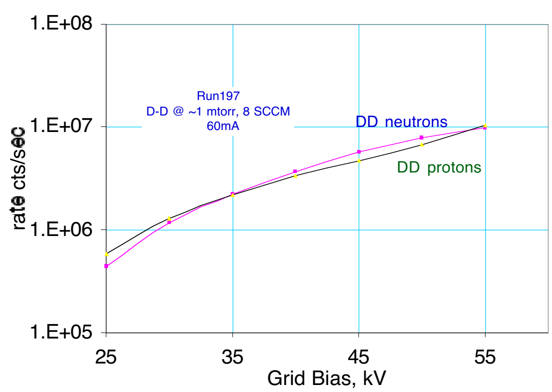

Figure 6. Fusion product rates vs. grid bias.

The highest steady-state D-D fusion neutron rate achieved was 4.9x10^7/s at 55 kV, 117 mA. This amounts to $\approx 10^8$ DD reactions per second. The reaction rate has a near linear dependency on the current at moderate pressures and grid potentials.

The D-D fusion reaction produces an equal number of 3 MeV protons and 2.45 MeV neutrons, so the detected rates of the protons and neutrons should be equal. The calibration depends on the proper calculation of the volume source in the truncated cone that the proton detector sees plus the cylindrical source of neutrons throughout the whole chamber. The fact that the calibrated rates are similar (Figure 6) confirms the volume source, charge exchange conditions.

Using a mixture of deuterium and ^{3}He gas to produce D^{3}He fusion, D-D fusion also takes place, producing 3 MeV protons along with the 14.7 MeV protons. The simultaneous detection of both of these protons is a valuable diagnostic, providing a measurement of the ratio between the D^{3}He and D-D fusion reactions that occur (Figure 7). At this grid voltage level, noise due to x-rays is starting to add to the D-D proton counts. It also clearly shows that the D^{3}He proton rate has surpassed the D-D proton rate.

This reaction ratio must be optimized to increase the production of 14.7 MeV protons. D^{3}He fusion can occur when a fast D ion or charge exchanged neutral hits a ^{3}He neutral, or a fast ^{3}He ion or charge exchanged neutral hits a D neutral. Deuterium is easier to ionize than helium-3, so the probable reaction occurs when a fast D ion or neutral hits a D or ^{3}He neutral.

As expected, the ratio of the two gas fuels has an influence on the reaction rates (Figure 8). This data set, recorded with the use of a RGA to monitor the fuel ratios, indicates that a ^{3}He to D ratio of 1 is optimal. Higher ratios would have a reduced density of deuterium ions, while a lower ratio would have a reduced density of helium-3 targets

The other main factor influencing the ratios of the reaction rates is the reaction cross section for a given kinetic energy of the ions. At higher energies, the D^{3}He cross-section exceeds the D-D value. Therefore, the D^{3}He to D-D reaction ratio should increase with increasing cathode voltage, which is confirmed by the experimental data in Figure 9. Comparing Figures 2 and 9 shows that the measured D-D to D^{3}He reaction rate ratio is consistent with the dominance of charge-exchange neutrals fusing with background neutrals over converged-core fusion.

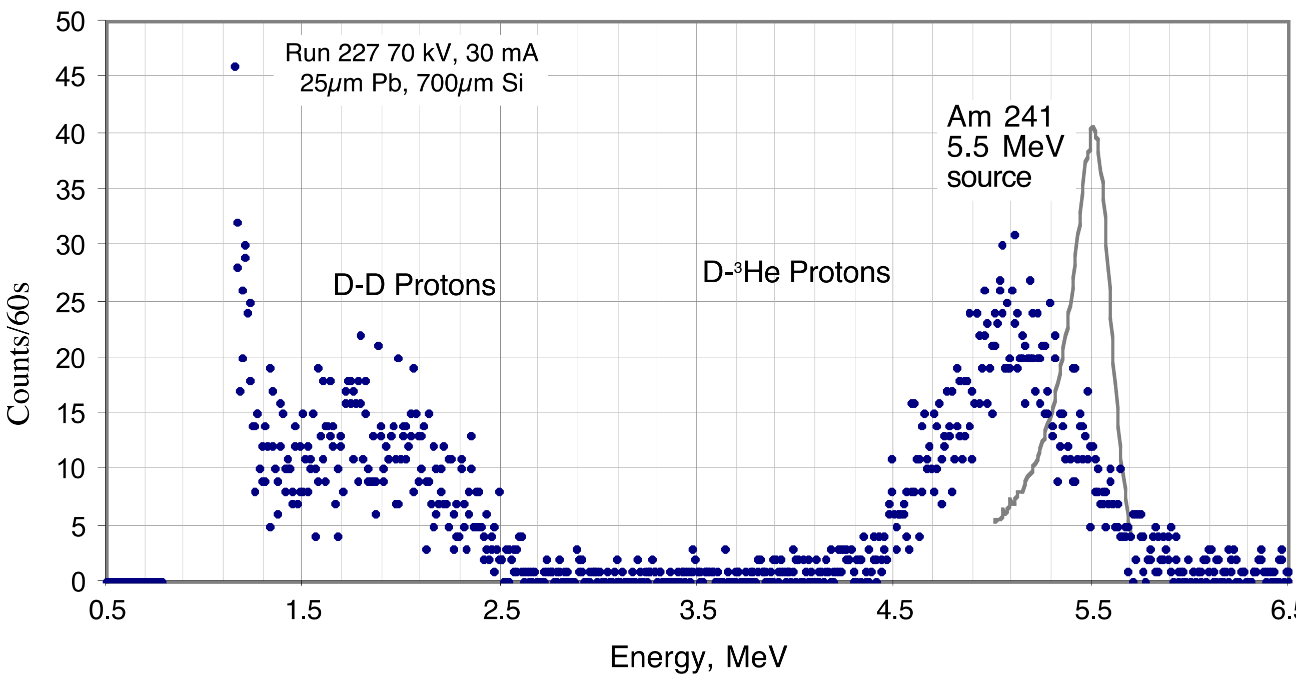

Figure 7. The energy deposited by D-D and D^{3}He protons in the Si detector agrees with theory.

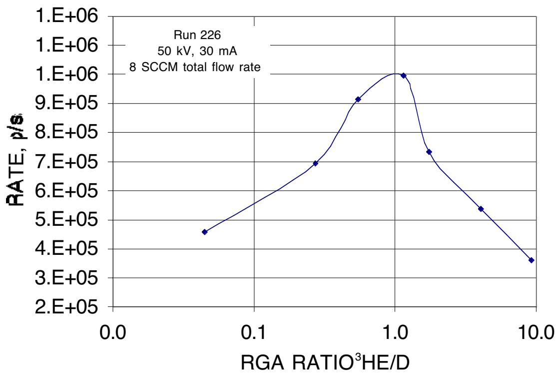

Figure 8. Fuel ratio vs. proton production.

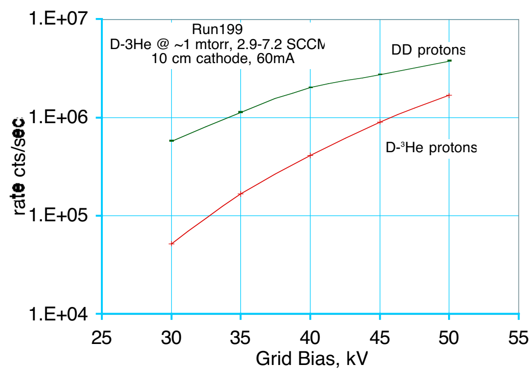

Figure 9. Fusion product rates vs. grid bias.

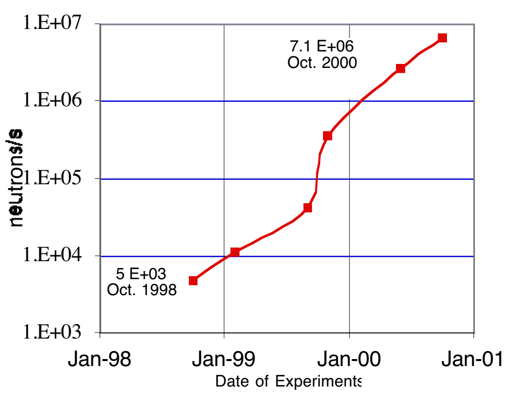

Figure 10. History of D^3He proton production.

The University of Wisconsin's IEC reactor was the first to achieve steady-state D^3He fusion[25] and has made great progress in increasing the production of protons from the D^3He reaction (Figure 10). The current record steady-state 14.7 MeV proton production is 7 x 10^6 protons/s at 70 kV, 30 mA.

V. CONCLUSIONS

Experiments at the University of Wisconsin Fusion Technology Institute have been successful in creating record steady-state D^3He fusion using its IEC fusion device. This fusion reaction, using the advanced fuel D^3He, produces 14.7 MeV protons that can be used in a variety of applications. Substantial progress in the fusion reaction rate of D^3He has been achieved, currently at 7 x 10^6 protons/s, as well as D-D fusion reaction rates. The fusion of other advanced fuels will be explored.

ACKNOWLEDGEMENTS

The authors would like to acknowledge that the FINDS Foundation, the Grainger Foundation, and Dr. Wilson Greatbatch funded this work. The authors would also like to acknowledge support from the University of Wisconsin-Madison.

REFERENCES

1. G.L. Kulcinski, "Near Term Commercial Opportunities from Long Range Fusion Research," *Fusion Technology* **30**, 411 (1996).
2. G.L. Kulcinski, "Non-Electric Applications of Fusion Energy—An Important Precursor to Commercial Electric Power," *Fusion Technology* **34**, 477 (1998).
3. G.L. Kulcinski, *Non-Electrical Power, Near Term Applications of Fusion Energy*, 8th Symposium on Fusion Engineering, IEEE #99CH37050 (1999).
4. J.F. Santarius, "Advanced-Fuel Heat Flux, Power Density, and Direct Conversion Issues," *Transactions of Fusion Technology* **27**, 567 (1995).
5. G.L. Kulcinski and J.F. Santarius, "New Opportunities for Fusion in the 21st Century–Advanced Fuels," 14th Topical Meeting, American Nuclear Society, Park City, Utah, Oct. 17-20, 2000.
6. J.F. Santarius, "Magnetic Fusion for Space Propulsion," *Fusion Technology* **21**, 1794 (1992).
7. E. Teller, et al., "Space Propulsion by Fusion in a Magnetic Dipole," *Fusion Technology* **22**, 82 (1992).
8. J.F. Santarius, "Field-Reversed Configurations for Space Propulsion," *31st AIAA Plasmadynamics and Lasers Conference*, #AIAA-2000-2269 (2000).
9. J.F. Santarius and B.G. Logan, "Generic Magnetic Fusion Rocket Model," *Journal of Propulsion and Power* **14**, 519 (1998).
10. P.T. Farnsworth, "Method and Apparatus for Producing Nuclear-Fusion Reactions," U.S. Patent #3,386,883 (1968).

11. R.L. Hirsch, "Inertial-Electrostatic Confinement of Ionized Fusion Gases," *Journal of Applied Physics* **38,** 4522 (1967).
12. G.H. Miley, et al., "Inertial-Electrostatic Confinement: An Approach to Burning Advanced Fuels," *Fusion Technology* **19**, 840 (1991).
13. Y. Gu, J.B. Javedani, and G.H. Miley, "A Portable Cylindrical Electrostatic Fusion Device for Neutronic Tomography," *Fusion Technology* **26**, 929 (1994).
14. M. Ohnishi, et al., "Correlation Between Potential Well Structure and Neutron Production in Inertial Electrostatic Confinement Fusion," *Nuclear Fusion* **37**, 611 (1997).
15. M. Ohnishi, et al., "Studies of Inertial-Electrostatic Confinement Fusion Neutron Source," *Fusion Technology* **34**, 1071 (1998).
16. Y. Gu and G.H. Miley, "Experimental Study of Potential Structure in a Spherical IEC Fusion Device," IEEE Transactions of Plasma Science, **28** **(2)** February 2000.
17. M. Rosenberg and N.A. Krall, "The Effect of Collisions in Maintaining a Non-Maxwellian Plasma Distribution in a Spherically Convergent Ion Focus," *Physics of Fluids* **B4**, 1788 (1992).
18. W.M. Nevins, "Can Inertial Electrostatic Confinement Work Beyond the Ion-Ion Collisional Time Scale?" *Physics of Plasmas* **2**, 3804 (1995).
19. T.H. Rider, "A General Critique of Inertial-Electrostatic Confinement Fusion Systems," *Physics of Plasmas* **2**, 1853 (1995).
20. L. Chacón, et al., "Energy Gain Calculations in Spherical Inertial Electrostatic Penning Fusion Systems Using a Bounce-Averaged Fokker-Planck Model," *Physics of Plasmas* (submitted).
21. R.W. Bussard, "Some Physics Considerations of Magnetic Inertial-Electrostatic Confinement: A New Concept for Spherical Converging-Flow Fusion," *Fusion Technology* **19**, 273 (1991).
22. Noah Hershkowitz, private communication.
23. T.A. Thorson, et al., "Convergence, Electrostatic Potential, and Density Measurements in a Spherically Convergent Ion Focus," *Physics of Plasmas* **4** , 4 (1997).
24. T.A. Thorson, et al., "Fusion Reactivity Characterization of a Spherically Convergent Ion Focus," *Nuclear Fusion* **38**, 495 (1998).
25. R.P. Ashley, et al., *D^3He Fusion in an Inertial Electrostatic Confinement Device,* 18th IEEE/NPSS Symposium on Fusion Engineering, IEEE #99CH37050 (1999).
26. M.J. Berger, J.S. Coursey, M.A. Zucker (1999) ESTAR, PSTAR, and ASTAR: Computer Programs for Calculating Stopping-Power and Range Tables for Electrons, Protons, and Helium Ions (version 1.21), [Online]. Available: http://physics.nist.gov/Star [2001 January 12]. National Institute of Standards and Technology, Gaithersburg, MD.